


Spin torque generated by valley Hall effect in WSe₂D. J. P. de Sousa,^{1,*} M. J. Sammon,¹ Raseong Kim²,² Hai Li²,² Ian A. Young,² and Tony Low^{1,†}¹*Department of Electrical and Computer Engineering, University of Minnesota, Minneapolis, Minnesota 55455, USA*²*Components Research, Intel Corporation, Hillsboro, Oregon 97124, USA* (Received 22 June 2022; revised 16 October 2022; accepted 1 November 2022; published 14 November 2022)

Monolayer transition metal dichalcogenides are promising materials for spintronics due to their robust spin-valley locked valence states, enabling efficient charge-to-spin conversion via the valley Hall effect with nonequilibrium spins possessing long spin diffusion lengths of hundreds of nanometers. In this paper, we show that the injection of a pure valley current, induced by the valley Hall effect in a WSe₂ monolayer, imparts a spin torque on the magnetization of an overlaid Fe or CoFe in a tunneling structure. The torque efficiency is found to be comparable to that in conventional perpendicular magnetic tunnel junctions and can be further optimized with the valley Hall angle in WSe₂. The valley nature of the spin torque gives rise to out-of-plane dampinglike torques in a current-in-plane configuration, vanishing charge transport perpendicular to the plane, as well as torque efficiency tunable through gating.

DOI: [10.1103/PhysRevB.106.184412](https://doi.org/10.1103/PhysRevB.106.184412)**I. INTRODUCTION**

The ability to electrically manipulate the magnetization of a ferromagnetic thin film with perpendicular magnetic anisotropy in an efficient manner is envisioned to enable unprecedented technological advances through the implementation of in-memory computing technologies [1–6]. Deterministic field-free switching of a perpendicular magnetization requires incident spin currents with a nonvanishing spin component aligned with the perpendicular anisotropy axis. State-of-the-art approaches to the generation of such out-of-plane spins include the charge-to-spin conversion through unconventional spin Hall effects in low-symmetry nonmagnets [7–11] and the injection of spins by additional ferromagnet layers in fully perpendicular magnetic tunnel junctions [1,12–15]. Recently, a new subfield of spintronics has emerged [16–19] which exploits the valley degree of freedom of electrons in two-dimensional materials. Here, we examine the spin torque generated through a valley polarization on an overlaid ferromagnet, and its efficiency in switching a perpendicular magnetization. Addressing this question is key in evaluating the potential of valley physics for spintronics.

In monolayer transition metal dichalcogenides (TMDs), the spin-orbit interaction induces a spin-valley locking, with K and K' valleys supporting opposite spin states as required by time-reversal symmetry. Spin-resolved photoemission spectroscopy measurements have revealed valley-dependent out-of-plane spin-polarized valence states in TMDs [20–24]. Subsequently, transport experiments unambiguously demonstrated that a flow of out-of-plane spins in WSe₂ monolayers can be electrically generated through the valley Hall effect

(VHE) [25], a topological Hall response driven by the finite and opposite Berry curvatures in the two valleys [25–29]. In these reports, an out-of-plane spin/valley polarization of 70% was observed at the edges of a p -doped monolayer WSe₂ due to VHE [29]. A similar electrically generated interfacial spin polarization of 38% was also observed in a WSe₂/graphene heterostructure [25]. Spin-valley locked states in TMDs are also long lived [30,31] with large out-of-plane spin diffusion lengths of hundreds of nanometers [27]. These features indicate the potential of spin-valley locking physics to enable unprecedented applications in spintronics.

In this paper, we address the feasibility of utilizing the spin-valley locking of TMDs to induce reversal of an adjacent perpendicular magnetization. By performing transport calculations on a TMD/insulator/ferromagnetic tunnel junction, we show the existence of a sizable spin torque (ST) acting on the magnetization of a Fe or CoFe slab originating solely from a nonequilibrium valley polarization in a WSe₂ monolayer. We found that the torque efficiency due to spin-valley locking depends sensitively on the WSe₂ doping levels and on the lattice misalignment with the ferromagnet and is comparable to that in a perpendicular magnetic tunnel junction. The fact that the ST arises from the flow of out-of-plane spins constitutes a mechanism suitable for switching a perpendicular magnetization. Our findings point toward the utilization of spin-valley locking physics of TMDs in efficient quantum spintronic devices.

II. THEORETICAL METHOD

Figure 1(a) displays a WSe₂/insulator/CoFe stack as a prototypical example of the tunneling junction studied in this paper. In this system, a nonequilibrium valley population induced in the WSe₂ portion underneath the CoFe slab gives rise to vertical tunneling valley currents. This situation can be realized by positioning the CoFe slab on one of the side arms

*sousa020@umn.edu

†tlow@umn.edu

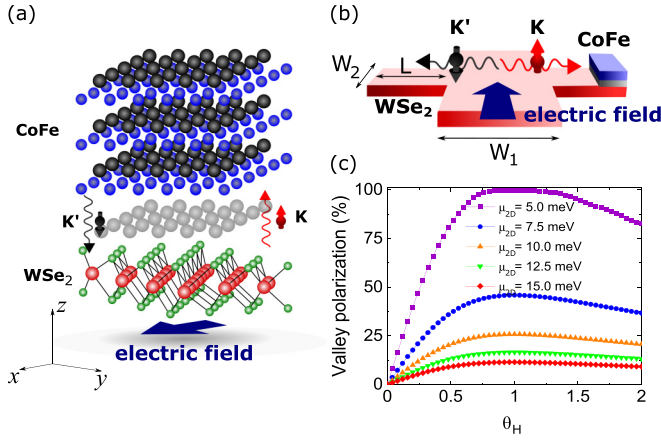


FIG. 1. (a) Representative WSe₂/insulator/CoFe tunnel junction with vertical tunneling valley/spin currents induced by an in-plane electric field in the WSe₂ monolayer. (b) The valley Hall effect causes a nonequilibrium valley imbalance in the transverse side arms of a WSe₂ crossbar in response to a longitudinal in-plane electric field. The induced valley voltage is optimized when the dimensions W_1 , W_2 , and L are smaller than the spin/valley diffusion length in WSe₂. (c) Field-induced nonequilibrium valley polarization in WSe₂ as a function of the valley Hall angle at several equilibrium WSe₂ doping levels μ_{2D} .

of the WSe₂ crossbar and taking advantage of the VHE to produce a local nonequilibrium valley density [see Fig. 1(b)]. The associated nonequilibrium valley chemical potential difference, $\delta\mu = \mu_K - \mu_{K'}$, is well described by the drift-diffusion approach [32], which renders

$$\delta\mu = \frac{eI}{\sigma_{xx}} \frac{\theta_H}{1 + \theta_H^2}, \quad (1)$$

where I is the electric field-accompanying in-plane charge current and θ_H the valley Hall angle of WSe₂, defined as $\theta_H = \sigma_H/\sigma_{xx}$ where σ_H and σ_{xx} are the valley Hall and longitudinal charge conductivities, respectively. Our drift-diffusion analysis indicates that Eq. (1) is the optimized valley potential induced by VHE in a crossbar geometry. The optimization takes place in the limit where the crossbar arm dimensions, W_1 , W_2 , and L , become smaller than the spin diffusion length in WSe₂, where $\delta\mu$ becomes independent of the crossbar dimensions. In the Supplemental Material, we present numerical results showing the validity of Eq. (1) and how the optimization comes about in the large spin-valley diffusion length limit [32,33]. The electric field is assumed to be applied along the x direction and the longitudinal charge conductivity is $\sigma_{xx} = (4e^2/h)(\eta\beta)^{-1} \ln[1 + \exp(\beta\mu_{2D})]$, where μ_{2D} characterizes the doping levels of WSe₂ and $\beta = 1/k_B T$, with k_B being the Boltzmann constant and T the temperature [34]. The valley polarization is defined as $(n_K - n_{K'})/(n_K + n_{K'}) \times 100\%$ with valley-dependent carrier density $n_{K(K')} = (m^*/\beta\pi\hbar^2) \ln[1 + \exp(\beta[\mu_{2D} \pm \delta\mu/2])]$ where m^* is the effective mass of the WSe₂ valence states.

Figure 1(c) reveals that the total electrically generated valley polarization induced at the side arms of the crossbar is a nonmonotonic function of θ_H with a maximum at $\theta_H \approx 1$ for all doping levels μ_{2D} . Similar nonmonotonic behavior

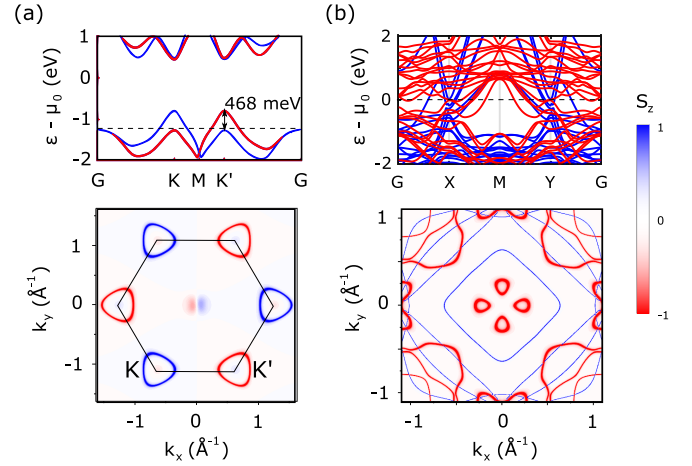


FIG. 2. The first-principles spin-resolved band structure (top panel) and spin density of states (bottom panel) of a WSe₂ monolayer and a 0.7-nm-thick CoFe slab are shown in (a) and (b), respectively. The horizontal dashed line in the band structure plots indicate the energy used in the corresponding spin density-of-states calculations. The valence states of WSe₂ display a valley-dependent out-of-plane spin polarization (S_z) that can be extracted through valley Hall effect [25].

was reported in Ref. [35]. Substantial valley polarizations are easily achieved at smaller μ_{2D} due to the fact that valley depopulation takes place with greater ease at lower μ_{2D} owing to the larger resistivity. The vertical flow of such nonequilibrium valley-polarized electrons can be addressed through a quantum mechanical tunneling approach, as described in the following.

We employ the Bardeen transfer Hamiltonian formalism [36,37] to describe the tunneling process between the WSe₂ monolayer and ferromagnetic thin film. In Bardeen's approach, quantum tunneling is treated perturbatively with transition rates being fully described by the electronic ground state of isolated contacts [38,39]. The electronic states were obtained with the pseudopotential/plane-wave method employed in QUANTUM ESPRESSO [40] and subsequently converted to maximally localized Wannier function basis with the WANNIER90 package [41]. Figures 2(a) and 2(b) show the spin-resolved band structure and spin density of states of a WSe₂ monolayer and a 0.7-nm-thick CoFe slab, respectively. The valence states of the WSe₂ monolayer display giant spin splittings of ≈ 468 meV, in agreement with previous results [20,23], with nonequivalent valleys K and K' hosting opposite out-of-plane spin polarizations. This strong spin-valley locking is better appreciated in the bottom panel of Fig. 2(a), where we show the momentum-resolved spin density of states for the energy indicated by the horizontal dashed line in the band structure plot. The Fermi level momentum-resolved spin density of states of the CoFe slab, shown at bottom panel of Fig. 2(b), indicates the presence of electron states throughout the whole Brillouin zone including momenta coinciding with the K and K' valleys. These finite vertical tunneling currents require momentum matched states in the two layers.

The spin-space components of the tunneling charge-current density read

$$J^{ss'} = \frac{e}{\hbar} \int d\epsilon \int \frac{d\mathbf{k}_T}{(2\pi)^2} \int \frac{d\mathbf{k}_B}{(2\pi)^2} [f(\mathbf{k}_T) - f(\mathbf{k}_B)] \times T^{ss'}(\epsilon, \mathbf{k}_T, \mathbf{k}_B), \quad (2)$$

where $f(\mathbf{k}_{T(B)}) = [1 + \exp(\beta[\epsilon - \mu(\mathbf{k}_{T(B)})])]^{-1}$ is the Fermi-Dirac distribution of the top (bottom) electrode and $T^{ss'}(\epsilon, \mathbf{k}_T, \mathbf{k}_B)$ are the spin space components of the momentum-dependent tunneling rates. The momentum-dependent chemical potentials are $\mu(\mathbf{k}_B) = \mu_0 + \delta\mu(\mathbf{k}_B)$ and $\mu(\mathbf{k}_T) = \mu_0$, where μ_0 is the equilibrium chemical potential of the whole structure and $\delta\mu(\mathbf{k}_B)$ equals $+\delta\mu/2$ ($-\delta\mu/2$) at the K (K') valley due to the VHE. The function $\delta\mu(\mathbf{k}_B)$ is related to the electronic properties of WSe₂ and applied in-plane current through Eq. (1).

The tunneling rate components appearing in Eq. (2) are

$$T^{ss'}(\epsilon, \mathbf{k}_T, \mathbf{k}_B) = 2\pi \sum_{n,m} |M_{nm}^{ss'}(\mathbf{k}_T, \mathbf{k}_B)|^2 \delta \times (\epsilon - \epsilon_{n\mathbf{k}_T}) \delta(\epsilon - \epsilon_{m\mathbf{k}_B}), \quad (3)$$

with matrix elements expressed in terms of the electronic eigenstates of isolated top and bottom electrodes through

$$M_{nm}^{ss'}(\mathbf{k}_T, \mathbf{k}_B) = \frac{\hbar^2}{2m} \int_{z_0} dS \left(\frac{\partial \psi_{n\mathbf{k}_T}}{\partial z} \psi_{m\mathbf{k}_B}^\dagger - \psi_{n\mathbf{k}_T} \frac{\partial \psi_{m\mathbf{k}_B}^\dagger}{\partial z} \right), \quad (4)$$

where the surface integral is performed halfway inside the barrier at z_0 and m is the effective mass of electrons in the insulating region [32]. We use the embedded Green's function formalism for computing the matrix element [37,42,43]. In the Supplemental Material [32] we show how this approach can be used to model tunneling through amorphous tunnel barriers, such as AlO_x and GdO_x or even highly disordered hexagonal boron nitride (hBN) multilayers. While the insulator description is phenomenological, our approach enables the treatment of tunneling through incommensurate contacts at arbitrary lattice misorientations, which is impractical through fully first-principles means by virtue of fundamental periodicity constraints.

The total tunneling charge-current and out-of-plane polarized spin currents are $J_c = \bar{J} + \Delta J \cos(\theta)$ and $Q^z = \bar{Q}^z + \Delta Q^z \cos(\theta)$, respectively, where θ is the angle between the magnetization of the ferromagnetic slab and the z axis. We have defined $\bar{J} = (J^{\uparrow\uparrow} + J^{\uparrow\downarrow} + J^{\downarrow\uparrow} + J^{\downarrow\downarrow})/2$, $\Delta J = (J^{\uparrow\uparrow} - J^{\uparrow\downarrow} - J^{\downarrow\uparrow} + J^{\downarrow\downarrow})/2$, $\bar{Q}^z = (\hbar/4e)[J^{\uparrow\uparrow} + J^{\uparrow\downarrow} - J^{\downarrow\uparrow} - J^{\downarrow\downarrow}]$, and $\Delta Q^z = (\hbar/4e)[J^{\uparrow\uparrow} - J^{\uparrow\downarrow} + J^{\downarrow\uparrow} - J^{\downarrow\downarrow}]$. The damping-like torque acting on the magnetization of the ferromagnetic slab is $\boldsymbol{\tau} = \tau \hat{\mathbf{m}} \times (\hat{\mathbf{m}} \times \hat{\mathbf{z}})$ where $\hat{\mathbf{m}}$ is the unit vector along the magnetization direction and $\tau = [Q^z(0) - Q^z(\pi)]/2 \rightarrow \tau = \Delta Q^z$ [44]. In the following, we discuss the main features of the ST as well as the tunneling charge and spin current originating from a valley polarization in the WSe₂.

III. RESULTS AND DISCUSSIONS

We initially take the zigzag direction of the WSe₂ monolayer to be aligned with the [100] direction of the Fe and CoFe

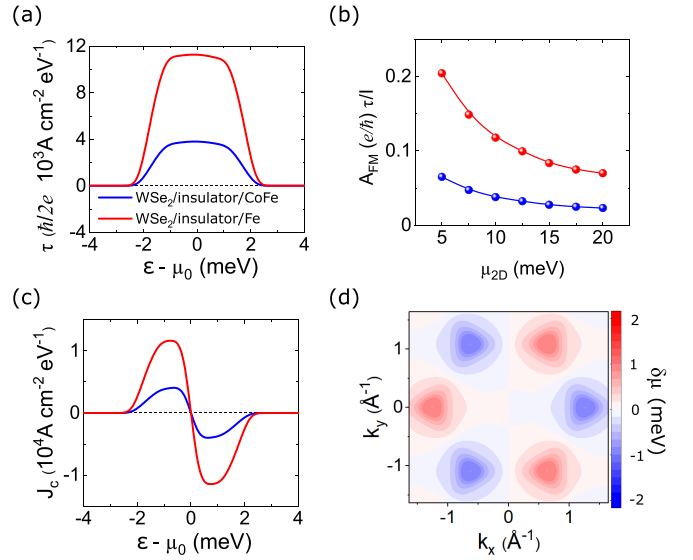


FIG. 3. (a) Energy-resolved spin torque acting on the magnetization of an Fe (red) and CoFe (blue) slab. The energies are measured in relation to the equilibrium chemical potential of the system μ_0 . (b) WSe₂ chemical potential dependence of the spin torque. Here, μ_{2D} characterizes the doping levels of WSe₂ only, i.e., the chemical potential of the ferromagnet is kept constant at μ_0 in these calculations. The energy-resolved tunneling charge current passing through the insulating barrier is shown in (c) for both systems. (d) Momentum-resolved nonequilibrium chemical potential of the WSe₂ monolayer.

slabs, an assumption that will be relaxed later. We assume $\theta_H = 0.4$ throughout [27]. Figure 3(a) displays the energy dependence of the dampinglike torque acting on the magnetization of a Fe (red curve) or CoFe (blue curve) slab. We have taken the in-plane charge current to be $I = 1 \mu\text{A}$ and the ST was evaluated at $\theta = \pi/2$, since its angular dependence is fully predetermined. As shown, all contributions to the ST take place within a small energy window around the equilibrium chemical potential, where states with energy above and below μ_0 contribute positively. Hence, a finite integrated ST acts on the magnetization of the ferromagnetic slab originating solely from the nonequilibrium valley-polarized electrons in the WSe₂ monolayer. Figure 3(a) also indicates a relatively stronger (weaker) ST in the WSe₂/insulator/Fe(CoFe) tunnel junction, which we will revisit later.

The ST efficiency in a ferromagnetic element of area $A_{\text{FM}} \approx 196 \text{ nm} \times 196 \text{ nm}$, defined as $\xi = A_{\text{FM}}(e/\hbar)\tau/I$, due to a valley polarization of 70% is found to be $\xi_{\text{CoFe}} \approx 0.07$ and $\xi_{\text{Fe}} \approx 0.2$ for CoFe and Fe, respectively, for typical WSe₂ hole concentrations of $p \approx 2.75 \times 10^{11} \text{ cm}^{-2}$. For the sake of comparison, the spin transfer torque efficiency in perpendicular magnetic tunnel junctions range in the interval 0.01–0.1 with a slight voltage dependence, as estimated from the typical critical switching current density 10^6 A/cm^2 and thermal stability factor of ≈ 60 [15,45,46]. Therefore, such valley-induced torque efficiency is large enough to excite the magnetization dynamics or reversal of a perpendicular ferromagnetic thin film. We also emphasize that the valley-induced torque efficiency can be further optimized with the

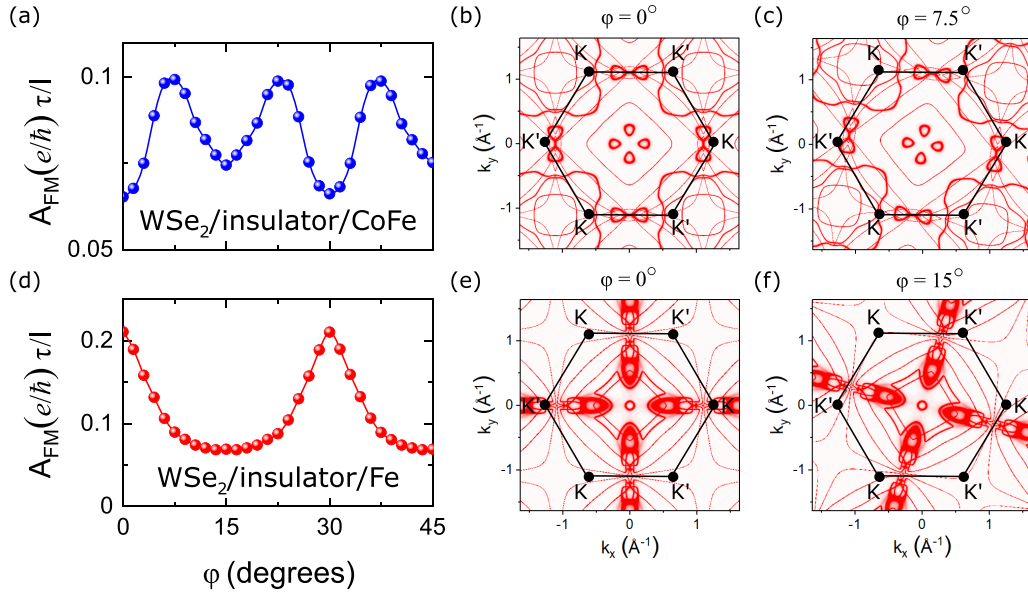


FIG. 4. Dependence of the spin torque efficiency due to a lattice misalignment. The lattice misalignment is quantified by the angle ϕ between the [100] direction of the ferromagnetic layer relative to the zigzag direction of the WSe₂ monolayer, which is held fixed along the x direction. (a) shows the angular dependence of the torque efficiency in the WSe₂/insulator/CoFe system while (b) and (c) show the momentum-resolved density-of-states map of the CoFe at $\phi = 0^\circ$ and $\phi = 7.5^\circ$, respectively. (d)–(f) display similar results but for the WSe₂/insulator/Fe system, where the misalignment angles in the two maps are taken to be $\phi = 0^\circ$ and $\phi = 15^\circ$. For visualization purposes, we superposed the hexagonal Brillouin zone of WSe₂, highlighting the valleys.

valley Hall angle and doping concentrations, as discussed next.

Our results also indicate that the ST efficiency depends sensitively on the doping levels of WSe₂, μ_{2D} , as measured from the valence band top. This is shown in Fig. 3(b) for the Fe (red symbols) and CoFe (blue symbols) cases. Here, the ST is a monotonically decreasing function of μ_{2D} with a stronger dependence at lower doping levels for both ferromagnetic slabs. This behavior is a signature of the valley polarization dependence of the ST and can be understood in the low-temperature limit as follows: The Fermi-Dirac distribution can be approximated as $f(\epsilon - \mu_{T(B)}) \approx \Theta(\mu_{T(B)} - \epsilon)$, where Θ is the Heaviside function, leading to $\tau \propto \delta\mu$. By explicitly writing $\delta\mu$ in terms of μ_{2D} through Eq. (1) we find $\tau/I \propto 1/\mu_{2D}$, in agreement with the behavior of Fig. 3(b). This result derives exclusively from the valley physics of the WSe₂ monolayer and suggests that the ST efficiency can be modulated through gating.

Figure 3(c) shows that for both ferromagnetic slabs, states with energies above and below μ_0 contribute oppositely to the vertical total charge-current density J_c . This is implied in the scenario of Fig. 1(a); the ST acting on the ferromagnet originates from an incoming flow of spin-up electrons and an outflow of spin-down electrons such that the net tunneling charge current vanishes while a net out-of-plane polarized spin current penetrates the ferromagnet. This is possible by the nonequilibrium valley-dependent chemical potential established in the WSe₂ monolayer as shown in Fig. 3(d), where the chemical potential of electrons with momenta at the vicinity of the K (K') is slightly lower (higher) than that of the ferromagnet, leading to a vertical outflow (inflow) of K (K') valley-polarized electrons.

To further explore the nature and behavior of the ST, we study how its magnitude is affected by a lattice misorientation. This is done by rotating the [100] orientation of the ferromagnetic layer by an angle ϕ with respect to the zigzag direction of the WSe₂ monolayer, which is maintained fixed along the x direction. The angular dependence of the torque efficiencies acting on the CoFe and Fe slabs are shown in Figs. 4(a) and 4(d), respectively. The results reveal an oscillatory behavior with a 30° period for both cases, where the maximum-to-minimum torque ratio, τ_{\max}/τ_{\min} , is approximately 1.5 and 3 for the CoFe and Fe cases, respectively. The stronger angular dependence in the Fe case is due to more Fermi-surface states at momenta coinciding with the K and K' valleys as compared to CoFe system. This is shown in Figs. 4(b) and 4(e), where we show the Fermi level momentum-resolved density of states of CoFe and Fe, respectively, at $\phi = 0^\circ$. The superposed hexagonal Brillouin zone of the WSe₂ monolayer highlights the location of K and K' valleys. As seen in Fig. 4(e), the two valleys located at $k_y = 0 \text{ \AA}^{-1}$ coincide with momentum space density-of-states hot spots of Fe, giving rise to a larger tunneling spin current. Such Fermi-surface matching is less ideal for the CoFe system. Figures 4(b) and 4(e) show the hot spot misalignments giving rise to the maximum ST efficiency in CoFe and Fe systems, respectively, while Figs. 4(c) and 4(f) display the configurations giving rise to the minimum ST efficiency (see Supplemental Material [32] for more discussion).

IV. CONCLUSIONS

We have shown that a valley Hall effect-induced nonequilibrium valley polarization in a WSe₂ monolayer results in a spin torque (ST) acting on the magnetization of a

ferromagnetic thin film in WSe_2 /insulator/ferromagnetic tunnel junctions. The valley-induced dampinglike torque arises from the flow of out-of-plane spin-polarized electrons and therefore is suitable for exciting magnetization dynamics of thin films with perpendicular magnetic anisotropy, an approach that does not require the presence of additional ferromagnetic elements or mirror-broken spin Hall materials. The valley-induced ST was shown to display an efficiency comparable to that in perpendicular magnetic tunnel junctions for typical valley polarizations reported from experiments, with further room for improvement through the valley Hall angle and doping concentrations in the WSe_2 monolayer, a feature that enables one to modulate the ST efficiency through

gating. Finally, we demonstrate how the lattice misalignment and different magnetic layers affect the spin torque efficiency.

ACKNOWLEDGMENTS

This material is based upon work supported by Intel Corporation from the University Center (Valleytronics) program. The authors acknowledge the Minnesota Supercomputing Institute (MSI) at the University of Minnesota for providing resources that contributed to the research results reported within this paper. URL: <http://www.msi.umn.edu>. We thank Punyashloka Debashis at Intel Corporation for helpful discussions.

- [1] H. Meng and J.-P. Wang, *Appl. Phys. Lett.* **88**, 172506 (2006).
- [2] S. Mangin, D. Ravelosona, J. A. Katine, M. J. Carey, B. D. Terris, and E. E. Fullerton, *Nat. Mater.* **5**, 210 (2006).
- [3] M. Gajek, J. J. Nowak, J. Z. Sun, P. L. Trouilloud, E. J. O'Sullivan, D. W. Abraham, M. C. Gaidis, G. Hu, S. Brown, Y. Zhu *et al.*, *Appl. Phys. Lett.* **100**, 132408 (2012).
- [4] D. Zhang, M. Bapna, W. Jiang, D. Sousa, Y.-C. Liao, Z. Zhao, Y. Lv, P. Sahu, D. Lyu, A. Naemi, T. Low, S. A. Majetich, and J.-P. Wang, *Nano Lett.* **22**, 622 (2022).
- [5] A. Sebastian, M. L. Gallo, R. K. Aljameh, and E. Eleftheriou, *Nat. Nanotechnol.* **15**, 529 (2020).
- [6] W. Zhang, B. Gao, J. Tang, P. Yao, S. Yu, M.-F. Chang, H.-J. Yoo, H. Qian, and H. Wu, *Nat. Electron.* **3**, 371 (2020).
- [7] D. MacNeill, G. M. Stiehl, M. H. D. Guimaraes, R. A. Buhrman, J. Park, and D. C. Ralph, *Nat. Phys.* **13**, 300 (2017).
- [8] F. Xue, C. Rohmann, J. Li, V. Amin, and P. M. Haney, *Phys. Rev. B* **102**, 014401 (2020).
- [9] S. Shi, J. Li, C.-H. Hsu, K. Lee, Y. Wang, L. Yang, J. Wang, Q. Wang, H. Wu, W. Zhang, G. Eda, G. Liang, H. Chang, and H. Yang, *Adv. Quantum Technol.* **4**, 2100038 (2021).
- [10] X.-G. Ye, P.-F. Zhu, W.-Z. Xu, N. Shang, K. Liu, and Z.-M. Liao, *Chin. Phys. Lett.* **39**, 037303 (2022).
- [11] D. J. P. de Sousa, P. M. Haney, J. P. Wang, and T. Low, *Phys. Rev. Appl.* **18**, 054020 (2022).
- [12] H. Suto, T. Nagasawa, T. Kanao, K. Yamada, and K. Mizushima, *Sci. Rep.* **9**, 19543 (2019).
- [13] D. J. P. de Sousa, P. M. Haney, D. L. Zhang, J. P. Wang, and T. Low, *Phys. Rev. B* **101**, 081404(R) (2020).
- [14] H. Liu, D. Bedau, J. Z. Sun, S. Mangin, E. E. Fullerton, J. A. Katine, and A. D. Kent, *J. Magn. Magn. Mater.* **358-359**, 233 (2014).
- [15] J. Z. Sun, *IBM J. Res. Dev.* **50**, 81 (2006).
- [16] H. Yuan, M. S. Bahramy, K. Morimoto, S. Wu, K. Nomura, B.-J. Yang, H. Shimotani, R. Suzuki, M. Toh, C. Kloc, X. Xu, R. Arita, N. Nagaosa, and Y. Iwasa, *Nat. Phys.* **9**, 563 (2013).
- [17] V. T. Renard, B. A. Piot, X. Waintal, G. Fleury, D. Cooper, Y. Niida, D. Tregurtha, A. Fujiwara, Y. Hirayama, and K. Takashina, *Nat. Commun.* **6**, 7230 (2015).
- [18] L. A. Benítez, J. F. Sierra, W. S. Torres, A. Arrighi, F. Bonell, M. V. Costache, and S. O. Valenzuela, *Nat. Phys.* **14**, 303 (2018).
- [19] R. Ahammed and A. De Sarkar, *Phys. Rev. B* **105**, 045426 (2022).
- [20] Z. Y. Zhu, Y. C. Cheng, and U. Schwingenschlögl, *Phys. Rev. B* **84**, 153402 (2011).
- [21] R. Suzuki, M. Sakano, Y. J. Zhang, R. Akashi, D. Morikawa, A. Harasawa, K. Yaji, K. Kuroda, K. Miyamoto, T. Okuda *et al.*, *Nat. Nanotechnol.* **9**, 611 (2014).
- [22] J. M. Riley, F. Mazzola, M. Dendzik, M. Michiardi, T. Takayama, L. Bawden, C. Granerød, M. Leandersson, T. Balasubramanian, M. Hoesch *et al.*, *Nat. Phys.* **10**, 835 (2014).
- [23] D. Xiao, G.-B. Liu, W. Feng, X. Xu, and W. Yao, *Phys. Rev. Lett.* **108**, 196802 (2012).
- [24] C. J. Ciccarino, T. Christensen, R. Sundararaman, and P. Narang, *Nano Lett.* **18**, 5709 (2018).
- [25] T. Y. T. Hung, A. Rustagi, S. Zhang, P. Upadhyaya, and Z. Chen, *InfoMat* **2**, 968 (2020).
- [26] K. F. Mak, K. L. McGill, J. Park, and P. L. McEuen, *Science* **344**, 1489 (2014).
- [27] Z. Wu, B. T. Zhou, X. Cai, P. Cheung, G.-B. Liu, M. Huang, J. Lin, T. Han, L. An, Y. Wang *et al.*, *Nat. Commun.* **10**, 611 (2019).
- [28] J. Lee, K. F. Mak, and J. Shan, *Nat. Nanotechnol.* **11**, 421 (2016).
- [29] E. Barré, J. A. C. Incorvia, S. H. Kim, C. J. McClellan, E. Pop, H.-S. P. Wong, and T. F. Heinz, *Nano Lett.* **19**, 770 (2019).
- [30] L. Yang, N. A. Sinitsyn, W. Chen, J. Yuan, J. Zhang, J. Lou, and S. A. Crooker, *Nat. Phys.* **11**, 830 (2015).
- [31] J. Kim, C. Jin, B. Chen, H. Cai, T. Zhao, P. Lee, S. Kahn, K. Watanabe, T. Taniguchi, S. Tongay, M. F. Crommie, and F. Wang, *Sci. Adv.* **3**, e170051 (2017).
- [32] See Supplemental Material at <http://link.aps.org/supplemental/10.1103/PhysRevB.106.184412> for more details on the theoretical model.
- [33] S. Hong, S. Sayed, and S. Datta, *IEEE Trans. Nanotechnol.* **15**, 225 (2016).
- [34] For the calculations presented in the main text, we assume $T = 1$ K for the temperature, $\eta = 0.1$ eV for the spectral broadening, and $I = 1$ μA for the in-plane electric field-accompanying charge current. Thermal smearing effects up to room temperature on the tunneling quantities are addressed in the Supplemental Material [32].
- [35] H. Li, D. E. Nikonov, C. C. Lin, K. Camsari, Y.-C. Liao, C.-S. Hsu, A. Naemi, and I. A. Young, *IEEE J. Explor. Solid-State Comput. Devices Circuits* **8**, 10 (2022).

- [36] J. Bardeen, *Phys. Rev. Lett.* **6**, 57 (1961).
- [37] D. Wortmann, H. Ishida, and S. Blügel, *Phys. Rev. B* **72**, 235113 (2005).
- [38] M. T. Greenaway, E. E. Vdovin, A. Mishchenko, O. Makarovskiy, A. Patanã, J. R. Wallbank, Y. Cao, A. V. Kretinin, M. J. Zhu, S. V. Morozov *et al.*, *Nat. Phys.* **11**, 1057 (2015).
- [39] R. M. Feenstra, D. Jena, and G. Gu, *J. Appl. Phys.* **111**, 043711 (2012).
- [40] P. Giannozzi, O. Andreussi, T. Brumme, O. Bunau, M. Buongiorno Nardelli, M. Calandra, R. Car, C. Cavazzoni, D. Ceresoli, M. Cococcioni *et al.*, *J. Phys.: Condens. Matter* **29**, 465901 (2017).
- [41] A. A. Mostofi, J. R. Yates, G. Pizzi, Y.-S. Lee, I. Souza, D. Vanderbilt, and N. Marzari, *Comput. Phys. Commun.* **185**, 2309 (2014).
- [42] J. Li, Y. Nie, K. Cho, and R. M. Feenstra, *J. Electron. Mater.* **46**, 2 (2017).
- [43] N. Prasad, G. W. Burg, K. Watanabe, T. Taniguchi, L. F. Register, and E. Tutuc, *Phys. Rev. Lett.* **127**, 117701 (2021).
- [44] I. Theodonis, N. Kioussis, A. Kalitsov, M. Chshiev, and W. H. Butler, *Phys. Rev. Lett.* **97**, 237205 (2006).
- [45] In these estimations, we assume $\alpha = 0.001$ is the intrinsic damping of the ferromagnetic slab.
- [46] A. Kalitsov, W. Silvestre, M. Chshiev, and J. P. Velev, *Phys. Rev. B* **88**, 104430 (2013).